

Rapid Commun. Mass Spectrom. 2014, 28, 691–698
(wileyonlinelibrary.com) DOI: 10.1002/rcm.6829

Infrared multiple-photon dissociation spectroscopy of deprotonated 6-hydroxynicotinic acid

Michael J. van Stipdonk^{1,2*}, Michael J. Kullman³, Giel Berden⁴ and Jos Oomens^{4,5}

¹Department of Chemistry and Biochemistry, Duquesne University, Pittsburgh, PA, USA

²Agilent Center of Excellence in Mass Spectrometry, Duquesne University, Pittsburgh, PA, USA

³Amun Enterprises, Wichita, KS, USA

⁴Radboud University Nijmegen, Institute for Molecules and Materials, FELIX Facility, Toernooiveld 7, 6525 ED Nijmegen, The Netherlands

⁵University of Amsterdam, Science Park 904, 1098 XH Amsterdam, The Netherlands

RATIONALE: Hydroxynicotinic acids (2-, 4-, 5- and 6-hydroxy) are widely used in the manufacture of industrial products, and hydroxypyridines are important model systems for study of the tautomerization of N-heterocyclic compounds. Here we determined the gas-phase structure of deprotonated 6-hydroxynicotinic acid (6OHNic).

METHODS: Anions were generated by electrospray ionization, and isolated and stored in a Fourier transform ion cyclotron resonance mass spectrometer. Infrared (action) spectra were collected by monitoring photodissociation yield versus photon energy. Experimental spectra were then compared with those predicted by density functional theory (DFT) and second-order Møller-Plesset (MP2) perturbation theory calculations.

RESULTS: For neutral 6OHNic, DFT and MP2 calculations strongly suggest that the 6-pyridone tautomer is favored when solvent effects are included. The lowest energy isomer of deprotonated 6OHNic, in the aqueous or gas phase, is predicted to be the 6-pyridone structure deprotonated by the carboxylic acid group.

CONCLUSIONS: The deprotonated, 6-pyridone structure is confirmed by comparison of the infrared multiple-photon photodissociation (IRMPD) spectrum in the region of 1100–1900 cm⁻¹ with those predicted using DFT and MP2 calculations. Copyright © 2014 John Wiley & Sons, Ltd.

In a recent study,^[1] we used the combination of ion-trap mass spectrometry, infrared multiple-photon photodissociation (IRMPD) spectroscopy and density functional theory (DFT) calculations to investigate of the structure of protonated 2-hydroxynicotinic acid and its dehydration product. DFT calculations suggested that an acylium ion (i.e. loss of H₂O from the acid group) is energetically more favored than a species generated by elimination of H₂O from the hydroxypyridine ring. Formation of the acylium product was confirmed by comparing the IRMPD spectrum with theoretical spectra from (DFT) harmonic calculations for several possible isomers. A thorough DFT study of the reaction dynamics suggested that the acylium ion is generated from the global minimum for the protonated precursor along a pathway that involves proton transfer from the hydroxypyridine ring and elimination of -OH from the acid group.

In the present study, our focus was on the deprotonated 6-hydroxynicotinic acid (6OHNic) ion. The hydroxynicotinic acids (2-, 4-, 5- and 6-hydroxy) are widely used in the

manufacture of industrial products,^[2–7] and 6OHNic is an important precursor to many modern insecticides. At a more fundamental level, the hydroxypyridines are important model systems for study of the tautomerization of N-heterocyclic compounds. Indeed calculations appear to suggest that 6OHNic can exist in its neutral form as hydroxypyridine or oxo/6-pyridone structures.^[8]

Infrared spectra of ionic species confined to the gas-phase environment of a mass spectrometer can be generated using the combination of tandem mass spectrometry and (wavelength-selective) IRMPD (for reviews, see^[9–12] and the literature cited therein). In the IRMPD spectroscopy experiment used in this work, ions are transferred from the solution phase to the solvent-controlled environment of an ion trap mass spectrometer using electrospray ionization (ESI). After transfer to the gas phase, ions are irradiated at mid-IR wavelengths using a free electron laser (FEL). When the FEL wavelength matches a vibrational fundamental, absorption of multiple photons raises the vibrational energy of the trapped ion to the dissociation threshold. An IR spectrum is generated by measuring the fragmentation induced by this process as a function of photon wavelength. Vibrational mode assignment and structural determination are performed with the assistance of frequencies predicted by DFT.

* Correspondence to: M. J. van Stipdonk, Department of Chemistry and Biochemistry, Duquesne University, Pittsburgh, PA, USA.
E-mail: vanstipdonkm@duq.edu

EXPERIMENTAL

ESI FT-ICR mass spectrometry

6-Hydroxynicotinic acid was purchased from Thermo Fisher (San Jose, CA, USA) and used as received. For the IRMPD studies, a stock solution (0.001 molar) was prepared in a 50:50 mixture of deionized water and methanol. Previously established methods specific to successful creation of gas-phase ions and complexes in our laboratory were used for the generation of ions and the subsequent collection of IRMPD spectra.^[13–17] Briefly, ESI was performed in the negative ion mode using a Micromass (now a component of Waters Corporation, Milford, MA, USA) Z-Spray source. Dry nitrogen (~80 °C) was used to assist in the desolvation process. Ions were injected into a home-built Fourier transform ion cyclotron resonance (FT-ICR) mass spectrometer described in detail elsewhere.^[18] Ions were accumulated for the duration of the previous FT-ICR cycle (approximately 5 s) in an external hexapole and injected into the ICR cell via a quadrupole deflector and an octapole RF ion guide. Instrument operating parameters, such as desolvation temperature, cone voltage, and ion accumulation and transfer optics voltages, were optimized to maximize formation of $[M-H]^-$ ions and transfer of the species to the ICR cell.

Infrared multiple-photon dissociation (IRMPD)

Infrared spectra were recorded by measuring the photodissociation yield as a function of photon wavelength. Precursor $[M-H]^-$ ions were irradiated using 15–30 FELIX macropulses (35 mJ per macropulse, 5 μ s pulse duration, FWHM bandwidth ~0.5% of central λ). In the IRMPD process, a photon is absorbed when the laser frequency matches a vibrational mode of the gas-phase ion and its energy is subsequently distributed over all vibrational modes by intramolecular vibrational redistribution (IVR). The IVR process allows the energy of each photon to be dissipated before the ion absorbs another, which leads to promotion of ion internal energy toward the dissociation threshold via multiple photon absorption.^[19] It is important to note that IR spectra obtained using IRMPD are comparable with those collected using linear absorption techniques.^[20,21] For these experiments, the FEL wavelength was tuned between 6.25 and 11.2 μ m in 0.04 to 0.1 μ m increments. The magnitude of product and undissociated precursor ions was measured using the excite/detect sequence of the FT-ICR mass spectrometer after each IRMPD step. The IRMPD yield was normalized to the total ion current, and linearly corrected for variations in laser power across the wavelength range scanned.

DFT geometry and frequency calculations

All calculations (DFT and MP2) were performed using the Gaussian 09 group of programs.^[22] The search for minima for neutral and deprotonated 6OHNic acid was initiated using relaxed scans of dihedral angles for different tautomers at the B3LYP/3-21G* level of theory. Structures were then subjected to full optimization using the same functional and the 6-311+G(d,p) basis set all atoms. As discussed below, four isomers for the deprotonated molecule were identified that were significantly lower in energy than several for which

a ring C-H proton was removed. The optimization of the higher energy species was not pursued further. For the six lowest energy structures for the neutral version of 6OHNic, and four lowest energy structures of the deprotonated molecule, the relative energies and vibrational frequencies for comparison with IRMPD spectra were determined for these species at the B3LYP/6-311+G(d,p), B3LYP/6-311+G(3df,3p), M06-2X/6-311+G(d,p) and MP2/6-311+G(d,p) level of theory. Scaling factors were chosen empirically by bringing the predicted stretching frequencies in the C=O region into agreement with the IRMPD spectrum.

Transition states for inter-conversion of isomers were calculated using the QST2 method and were confirmed by the presence of a single imaginary frequency. As discussed below, the photodissociation pathway for deprotonated 6OHNic was loss of CO₂. For several isomers, CO₂ loss involves direct cleavage of the 6-pyridone ring C and the carboxylate group. However, for precursor species with a carboxylic acid group, loss of CO₂ requires intramolecular H atom transfer. The transition state for this process was also investigated using DFT and the QST2 approach. Where necessary, intrinsic reaction coordinates were performed to confirm that the identified transition states bridged the appropriate minima.

To determine the influence of solvent on the preference of respective neutral and deprotonated structures of 6OHNic, calculations (B3LYP, M06-2X and MP2) were also calculated with the Polarizable Continuum Model (PCM) using the integral equation formalism variant (referred to as IEFPCM in the Gaussian package). Solvent-phase calculations were set up and run using the IEFPCM setting and water as solvent in the solvation menu of the calculation set-up window in the GaussView 5.0.9 program (Gaussian Inc., Wallingford, CT, USA).

RESULTS AND DISCUSSION

Predicted structures of neutral and deprotonated 6OHNic

In a previous study, Santos and coworkers investigated the relationship between energetics and structure for 2-, 4-, 5-, and 6-hydroxynicotinic and 5-chloro-6-hydroxynicotinic acid using a combination of experimental and theoretical methods.^[8] Based on crystal structures determined by single crystal X-ray diffraction, 6OHNic, along with others in the general group, was found to crystallize as the oxo (6-pyridone) tautomer. This conclusion was supported by the observation of characteristic N-H and C_{ring}=O stretches in the FT-IR spectra of the respective compounds. More importantly, however, theoretical calculations carried out at the G3MP2 and CBS-QB3 levels of theory suggested that in the gas phase 2OHNic favors the oxo/6-pyridone form and that there is no strong preference for one or the other tautomer in the case of 6OHNic.

Structures for neutral 6OHNic that were identified as minima in our present study are provided in Fig. 1. The calculated energies of the species are provided in Table 1. Two of the minima are 6-pyridone tautomers (**6OHNic_1** and **6OHNic_2**) which differ only in the relative orientations of the carboxylic acid group with respect to the ring N atom. The remaining four isomers (**6OHNic_3** through **6OHNic_6**)

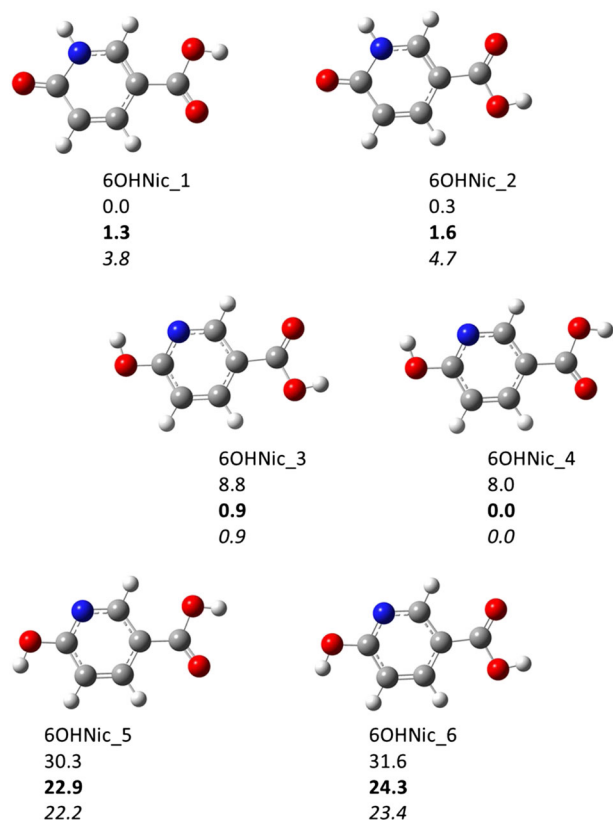


Figure 1. Predicted conformations for neutral 6OHNic. Relative energies are provided in Table 1. In the figure, relative energies at the B3LYP/6-311+G(d,p), M06-2X/6-311+G(d,p) and MP2/6-311+G(d,p) levels of theory are shown in plain, bold and italicized text, respectively.

are variations of the 6-hydroxypyridine tautomer, with the principal difference being the relative orientations of the carboxylic acid and ring -OH groups.

At the B3LYP/6-311+G(d,p) level of theory, the 6-pyridone structures (**6OHNic_1** and **6OHNic_2**) are favored over the hydroxypyridine isomers (**6OHNic_3** through **6OHNic_6**) by 8 to 30 kJ/mol, with the least energetically favorable conformations being those in which the ring -OH proton is positioned away from the ring N atom. For either tautomer, 6-pyridone versus hydroxypyridine, isomers that differ in the orientation of the carboxylic group lie within 2 kJ/mol from each other and are thus within the error typically associated with the DFT calculations. Structures **6OHNic_1** and **6OHNic_2** lie 1.3 to 1.6 kJ/mol in energy higher than structures **6OHNic_3** and **6OHNic_4** at the M06-2X/6-311+G(d,p) level of theory, but this difference is again probably within the error of the calculations. Similar results were obtained at the MP2/6-311+G(d,p) level of theory, with structures **6OHNic_3** and **6OHNic_4** favored over **6OHNic_1** and **6OHNic_2** by 3.8–4.7 kJ/mol. With the small differences in relative energy between the 6-pyridone and hydroxypyridine tautomers obtained here, our results are in general agreement with the earlier G3MP2 investigation, in which the conclusion drawn was that there is no strong preference for either the hydroxypyridine or 6-pyridone structures in the gas phase.

The minima identified for deprotonated 6OHNic are shown in Fig. 2 and the relative energies of the respective structures are provided in Table 2. The lowest energy isomer, regardless of the level of theory, was structure **6OHNic_dp2**, which is formally the 6-pyridone tautomer deprotonated at the carboxylic acid group. At the B3LYP/6-311+G(d,p) level of theory, the hydroxypyridine tautomer deprotonated at the carboxylic acid group, species **6OHNic_dp3**, is nearly 23 kJ/mol higher in energy. The differences in energy between the two structures at the M06-2X and MP2 levels of theory were 13.0 and 5.7 kJ/mol, respectively.

The lowest energy isomer in which the proton is formally eliminated from the 6-pyridone/hydroxypyridine group, structure **6OHNic_dp1**, is less favored by ~9–4 kJ/mol, depending on the level of theory. In general, structures in

Table 1. Calculated energies for neutral 6OHNic. Electronic and zero-point energies are in units of Hartree

B3LYP/6-311+G(d,p)	E	ZPE	E + ZPE	ΔE (kJ/mol)
6OHNic_1	-512.254063	0.108186	-512.145877	0.0
6OHNic_2	-512.254048	0.108272	-512.145776	0.3
6OHNic_3	-512.250574	0.108055	-512.142519	8.8
6OHNic_4	-512.250903	0.108065	-512.142838	8.0
6OHNic_5	-512.242006	0.107662	-512.134344	30.3
6OHNic_6	-512.241463	0.107627	-512.133836	31.6
M06-2X/6-311+G(d,p)	E	ZPE	E + ZPE	ΔE (kJ/mol)
6OHNic_1	-512.052355	0.109706	-511.942649	1.3
6OHNic_2	-512.052310	0.109759	-511.942551	1.6
6OHNic_3	-512.052569	0.109761	-511.942808	0.9
6OHNic_4	-512.052872	0.109729	-511.943143	0.0
6OHNic_5	-512.043942	0.10952	-511.934422	22.9
6OHNic_6	-512.043407	0.109513	-511.933894	24.3
MP2/6-311+G(d,p)	E	ZPE	E + ZPE	ΔE (kJ/mol)
6OHNic_1	-510.899265	0.106422	-510.792843	3.8
6OHNic_2	-510.899092	0.106594	-510.792498	4.7
6OHNic_3	-510.900809	0.106888	-510.793921	0.9
6OHNic_4	-510.901173	0.106897	-510.794276	0.0
6OHNic_5	-510.892242	0.106416	-510.785826	22.2
6OHNic_6	-510.891711	0.106336	-510.785375	23.4

which the proton was eliminated from the C atoms of the pyridine/hydroxypyridine ring range from ~80 to 240 kJ/mol higher in energy than **6OHNic_dp2**.

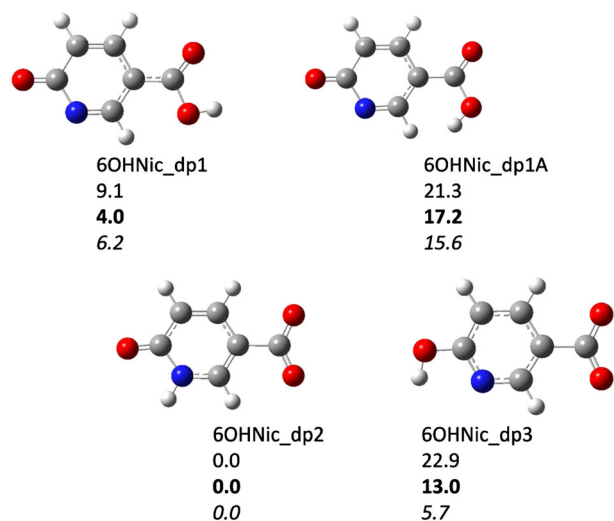


Figure 2. Predicted structures for deprotonated 6OHNic. Relative energies are provided in Table 2. In the figure, relative energies at the B3LYP/6-311+G(d,p), M06-2X/6-311+G(d,p) and MP2/6-311+G(d,p) levels of theory are shown in plain, bold and italicized text, respectively.

We were also interested in the barriers for isomerization of deprotonated 6OHNic. The barrier calculated for conversion of **6OHNic_dp2** into **6OHNic_dp3** (Supplementary Fig. S1, Supporting Information), which represents isomerization to the hydroxypyridine tautomer, is ~147 kJ/mol and probably reflects the fact that the proton transfer step requires a suprafacial 1-3 proton shift. The high barrier also suggests that interconversion between tautomers of the anion does not occur in the gas phase.

The DFT and MP2 calculations suggest that the energetically most favored structures of neutral and deprotonated 6OHNic, in the gas phase, feature a 6-pyridone structure, and for the anion, deprotonation occurs at the carboxylic acid group. However, the energy differences are not large compared with the expected error of the calculations of a few kJ/mol. To probe further the most likely solution-phase conformation of the neutral molecule, and the favored deprotonated molecule conformation in solution and the gas phase, we performed calculations with solvent effects included. As noted in the Experimental section, the condensed phase calculations were performed using the IEFPCM model with water as solvent. The relative energies for the respective neutral and deprotonated species generated using the IEFPCM method are included in Supplementary Tables S1 and S2, respectively (Supporting Information).

When solvent is considered, the differences in relative energy change significantly. For neutral 6OHNic, species **6OHNic_1** and **6OHNic_2** are favored over the other isomers

Table 2. Calculated energies for deprotonated 6OHNic, transition states for isomerization and for product ions generated by loss of CO₂. Electronic and zero-point energies are in units of Hartree

B3LYP/6-311 + G(d,p)	E	ZPE	E + ZPE	ΔE (kJ/mol)
6OHNic_dp1	-511.710322	0.093992	-511.616329	9.1
6OHNic_dp1A	-511.705230	0.093563	-511.611667	21.3
6OHNic_dp2	-511.714554	0.094761	-511.619793	0.0
6OHNic_TSdp2_dp3	-511.6531541	0.089504	-511.5636501	147.4
6OHNic_dp3	-511.705529	0.094474	-511.611055	22.9
6OHNic_dp1_prod1	-323.048860	0.078678	-322.970182	37.8
6OHNic_dp2_prod1	-322.987823	0.078752	-322.909071	198.2
6OHNic_dp3_prod1	-322.975701	0.07849	-322.897211	229.4
CO ₂	-188.646915	0.011688	-188.635227	
M06-2X/6-311 + G(d,p)	E	ZPE	E + ZPE	ΔE (kJ/mol)
6OHNic_dp1	-511.510776	0.095611	-511.415165	4.0
6OHNic_dp1A	-511.505621	0.095512	-511.410109	17.2
6OHNic_dp2	-511.512791	0.096118	-511.416673	0.0
6OHNic_dp3	-511.507811	0.096074	-511.411737	13.0
6OHNic_dp1_prod1	-322.824755	0.078666	-322.746089	37.5
6OHNic_dp2_prod1	-322.764320	0.078674	-322.685646	196.2
6OHNic_dp3_prod1	-322.752515	0.07852	-322.673995	226.8
CO ₂	-188.559275	0.012074	-188.547201	
MP2/6-311 + G(d,p)	E	ZPE	E + ZPE	ΔE (kJ/mol)
6OHNic_dp1	-510.355316	0.093442	-510.261874	6.2
6OHNic_dp1A	-510.351919	0.093606	-510.258314	15.6
6OHNic_dp2	-510.357803	0.093549	-510.264254	0.0
6OHNic_dp3	-510.355626	0.093554	-510.262072	5.7
6OHNic_dp1_prod1	-322.137916	0.078043	-322.059873	24.7
6OHNic_dp2_prod1	-322.076175	0.078476	-321.997699	187.9
6OHNic_dp3_prod1	-322.071906	0.078533	-321.993373	199.3
CO ₂	-188.206558	0.01157	-188.194988	

by 11–34 kJ/mol. For the deprotonated species, structure **6OHNic_dp2** is favored by 4–40 kJ/mol over the other possible tautomers in their respective isomeric forms. These energy differences lie beyond the error expected for the calculations. Therefore, our computational data suggest that **6OHNic** in aqueous solution is primarily the 6-pyridone tautomer, which deprotonates to generate the anion by elimination of the proton from the carboxylic acid group.

IRMPD of deprotonated **6OHNic**

To further test the hypothesis that the preferred structure for the **6OHNic** anion is the 6-pyridone tautomer, deprotonated at the carboxylic acid, we turned next to IRMPD spectroscopy. As noted earlier, elimination of CO_2 from deprotonated **6OHNic** was used as the photodissociation channel to record the IRMPD spectrum of the anion. The IRMPD spectrum of deprotonated **6OHNic** is shown in Fig. 3 (a). The vibrational spectra predicted at the B3LYP/6-311 + G(d,p) level of theory are compared with the IRMPD spectra in Figs. 3(b)–3(e) for the four lowest-energy isomers identified by DFT (structures **6OHNic_dp1**, **6OHNic_dp1A**, **6OHNic_dp2** and **6OHNic_dp3**, respectively). The best agreement between the theoretical and the IRMPD spectra is for **6OHNic_dp2**, consistent with the fact that this species is predicted to be lowest in energy by DFT and MP2 calculations and the IEFPCM model.

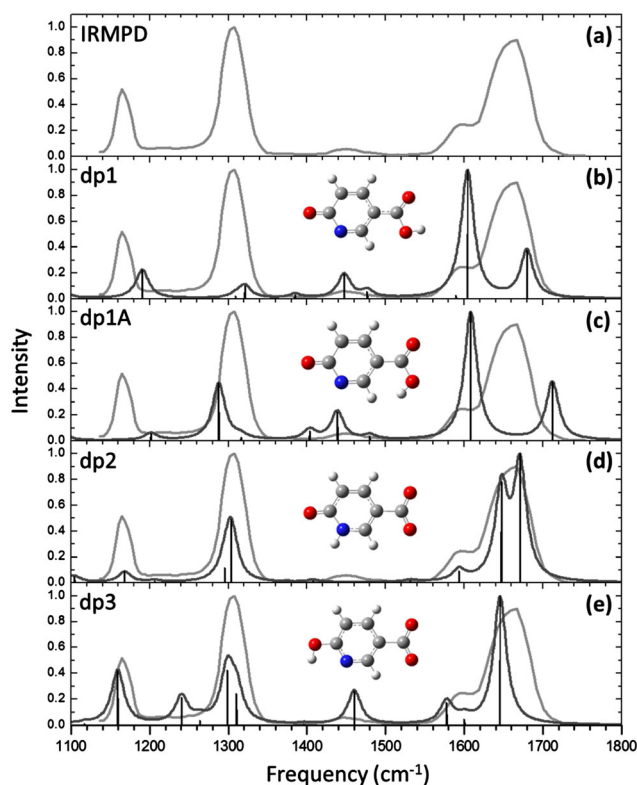


Figure 3. Comparison of (a) IRMPD spectrum for deprotonated **6OHNic** with predicted spectra for: (b) **6OHNic_dp1**, (c) **6OHNic_dp1A**, (d) **6OHNic_dp2**, and (e) **6OHNic_dp3**. Harmonic frequency calculations performed at the B3LYP/6-311 + G(d,p) level of theory. Frequencies scaled by a factor of 0.98.

Based on comparison with the predicted vibrations, the large absorption in the IRMPD spectrum at 1620–1700 cm^{-1} is assigned to two modes that are not resolved. The first is predicted at $\sim 1660 \text{ cm}^{-1}$ and corresponds to the stretch of the 6-pyridone C=O group coupled to ring C-H and N-H wag motions. The second absorption is predicted at $\sim 1640 \text{ cm}^{-1}$ and is assigned to the antisymmetric stretch of the free carboxylate group. A small shoulder to the low-frequency side is observed at $\sim 1590 \text{ cm}^{-1}$ and is assigned to coupled ring C-C stretches and C-H rocking modes. The relatively weak absorption observed at $\sim 1450 \text{ cm}^{-1}$ is assigned to the N-H wag of the pyridone group. The intense absorption at *ca* 1310 cm^{-1} is assigned to a symmetric carboxylate stretching mode. The other absorption observed at 1160 cm^{-1} corresponds to coupled ring C-H and N-H wag motion.

A quick survey of the predicted spectra generated using a larger basis set, a different functional or model was performed. In general, no significant change to the predicted spectra for the lowest energy isomers, or the agreement with the experimental IRMPD spectrum, was achieved using the B3LYP functional and the 6-311++G(3df,3p) basis set (Supplementary Fig. S2, Supporting Information). In addition, only modest changes to the predicted positions or intensities of vibrational frequencies were observed when the M06-2X functional was used in DFT, or MP2 calculations were used, both with the 6-311 + G(d,p) basis set (Supplementary Fig. S3, Supporting Information).

Despite the good general agreement between the IRMPD spectrum and the predicted frequencies for structure **6OHNic_dp2**, the vibrations predicted for the **6OHNic_dp1** are in reasonable agreement when considering just the positions of the respective absorptions. We note, though, that the predicted relative intensities of the vibrations are in poor agreement with the IRMPD spectrum. For **6OHNic_dp1**, the carboxylic acid and 6-pyridone C=O stretches are predicted to appear at ~ 1680 and 1600 cm^{-1} , respectively. Both are within the broad absorption observed in the IRMPD spectrum between 1560 and 1720 cm^{-1} . In addition, the small, broad absorption in the IRMPD spectrum matches well the position of two vibrations predicted to appear in the spectrum of **6OHNic_dp1** at ~ 1440 and 1480 cm^{-1} . These correspond to different combinations of coupled ring C-C stretches and C-H rocks. The absorption predicted to appear at $\sim 1290 \text{ cm}^{-1}$ in the theoretical spectrum of **6OHNic_dp1** corresponds to the acid CO-H bend.

The results obtained here for **6OHNic** can be compared with those for a larger group of free carboxylates that have been characterized by IRMPD spectroscopy. For example, the peak positions for the symmetric and antisymmetric carboxylate stretches for acetate are 1305 and 1590 cm^{-1} , respectively.^[23] For propionate, the carboxylate stretching modes were observed at 1305 and 1600 cm^{-1} . A more important comparison is perhaps with benzoate, for which the symmetric and antisymmetric carboxylate stretch modes were observed at 1626 and 1311 cm^{-1} , respectively.^[24] Therefore, despite the fact that the pyridone C=O stretch is not resolved in the present case from the antisymmetric carboxylate stretch, the general features of the IRMPD spectrum are consistent with those expected for free carboxylates in the gas phase. This provides further support to our hypothesis that the preferred structure of deprotonated **6OHNic**, at least in the gas phase, is that of a 6-pyridone tautomer as a carboxylate.

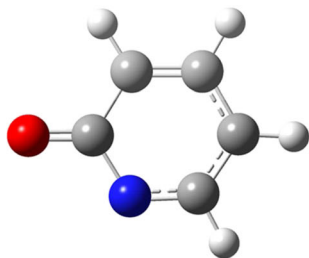
Fragmentation energetics

As noted above, the photodissociation signal used to generate the IRMPD spectrum was loss of CO₂. Structures **6OHNic_dp2** and **6OHNic_dp3** can eliminate CO₂ by direct cleavage of the C_{ring}-CO₂ bond, and the barrier for the pathway is expected to be the overall endothermicity of the reaction, i.e. there is no reverse barrier. The minima identified by DFT for the products generated by elimination of CO₂ from **6OHNic_dp1**, **6OHNic_dp2** and **6OHNic_dp3** are shown in Fig. 4, with the relative energies for the same species provided in Table 2. The CO₂-loss product from **6OHNic_dp1A** is identical to that for **6OHNic_dp1**. The reaction energies for CO₂ loss from structures **6OHNic_dp2** and **6OHNic_dp3** are estimated to be 198.2 and 206.4 kJ/mol based on simple differences in electronic energy between products and precursors.

Interestingly, the lowest energy (potential) photodissociation product is the one derived from **6OHNic_dp1**. However, loss of CO₂ from this species requires proton transfer from the carboxylic acid moiety to the ring through a reaction pathway shown in Fig. 5. This pathway is expected to be energetically and entropically less favored than the direct elimination of CO₂ from the other isomers. Based on DFT calculations, isomerization of **6OHNic_dp1** to **6OHNic_dp1A** is found to

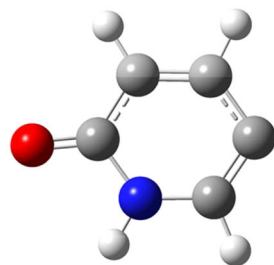
6OHNic_dp1_prod1

37.8
37.5
24.7



6OHNic_dp2_prod1

198.2
196.2
187.9



6OHNic_dp3_prod1

229.4
226.8
199.3

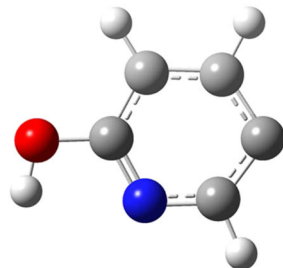


Figure 4. Possible structures for product ions generated by loss of CO₂ from deprotonated 6OHNic. Relative energies are provided in Table 2. In the figure, relative energies at the B3LYP/6-311 + G(d,p), M06-2X/6-311 + G(d,p) and MP2/6-311 + G(d,p) levels of theory are shown in plain, bold and italicized text, respectively.

proceed through a bond-rotation transition state with a barrier of 44.9 kJ/mol. The transfer of H from the carboxylic acid to the 6-pyridone ring and loss of CO₂ is energetically more costly, and occurs in a concerted step through a distorted four-center transition state with a relative energy of ~189 kJ/mol. The transfer process furnishes an ion-molecule complex between 6-pyridone and CO₂ with a relative energy of 29.2 kJ/mol relative to **6OHNic_dp1**.

Moving again to the discussion of likely solution- and gas-phase conformations of deprotonated 6OHNic, the comparison between IRMPD and DFT calculations strongly suggests that deprotonated 6OHNic has the conformation

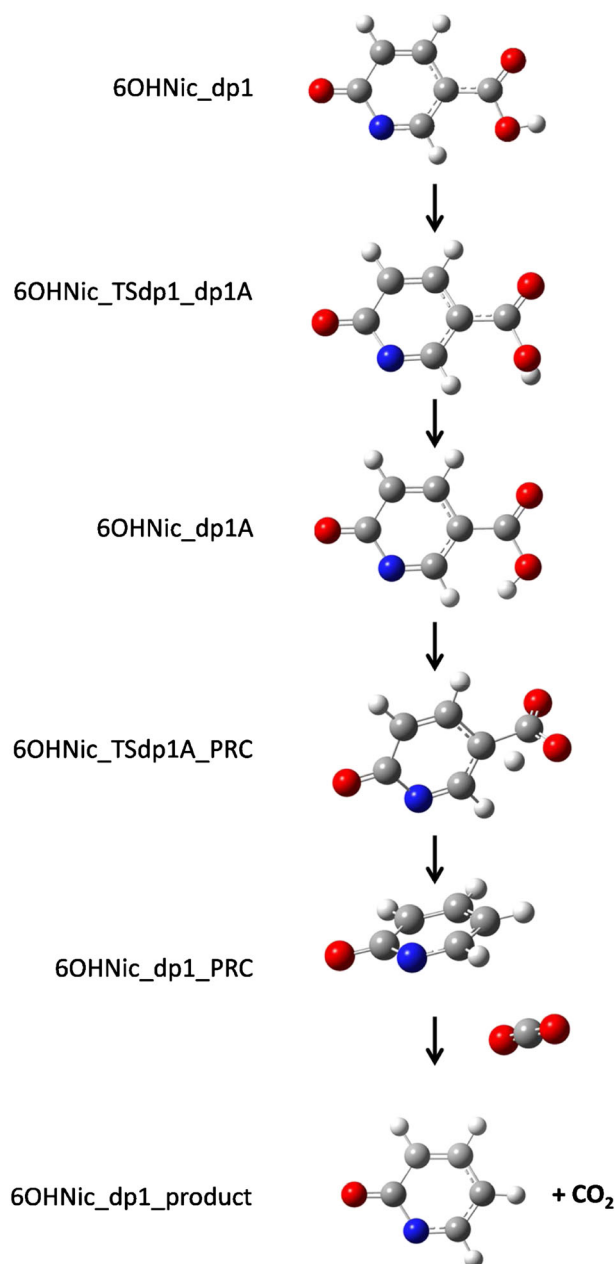


Figure 5. Pathway for elimination of CO₂ from deprotonated 6OHNic structure dp1. Calculations performed at the B3LYP/6-311 + G(d,p) level of theory.

6OHNic_dp2 because the relative positions and intensities of the predicted vibrations are in excellent agreement with the IRMPD spectrum. Confidence in the correct assignment of the structure to that of the 6-pyridone tautomer with the carboxylate group is increased when considering the fact that **6OHNic_dp2**, **6OHNic_1** and **6OHNic_2** (the neutral precursors) are calculated to be significantly lower in energy than the other isomers in solution. In addition, fragmentation of **6OHNic_dp1** or **6OHNic_dp1A**, to the extent that they would be present in the ion population, must involve elimination of CO₂ (the photodissociation channel observed) through an entropically less favored pathway with a barrier comparable with the dissociation energy of **6OHNic_dp2** and **6OHNic_dp3**.

CONCLUSIONS

For both neutral and deprotonated 6OHNic, DFT and MP2 calculations suggest that a 6-pyridone structure is favored over the hydroxypyridine tautomer, although the differences in energy between the various isomers were small if not within the error typically associated with the calculations. When the calculations were performed with solvent effects included using the IEFPCM model, more significant differences in energy were found that strongly suggest that the 6-pyridone tautomer is favored in aqueous solution. The lowest energy isomer of deprotonated 6OHNic, in the aqueous or gas phase, is predicted to be the 6-pyridone structure deprotonated by the carboxylic acid group. Strong supporting evidence for the hypothesis that deprotonated 6OHNic is a 6-pyridone tautomer with carboxylate was provided by a comparison of predicted frequencies for the respective isomers with the IRMPD spectrum in the region of 1100–1800 cm⁻¹. In particular, closely spaced C=O stretches for the free carboxylate and pyridine group are reproduced well by DFT and MP2 calculations.

Our results can be added to those revealed in several prior gas-phase, including IRMPD, studies of the structures of molecules that contain more than one acidic functional group. For example, focus has been placed on the conjugate base of 4-hydroxybenzoic acid (4HBA).^[25–31] While phenol is less acidic than benzoic acid,^[28] the proton on the ring-hydroxyl group of 4HBA is more acidic than the carboxy proton because of resonance stabilization and enhanced charge delocalization in the phenoxide structure.^[27,29] However, the carboxylate isomer of deprotonated 4HBA is favored in aqueous solution^[26] due to stabilization by hydrogen-bonding interactions. Indeed, IRMPD spectroscopy has shown that deprotonated 4HBA (and related species^[32]) adopts different structures in different ESI solvents and that the carboxylate solution-phase structure is easily transferred to the gas phase, where it is a kinetically stabilized structure high above the thermodynamic minimum.^[25]

While in the present case there is no strong difference between the different isomeric structures of deprotonated 6OHNic when calculations are performed for the gas phase, our results show that the IRMPD results can be rationalized, and the assignment of a most-probable 6-pyridone/carboxylate structure made, when calculations in solution are also performed.

Acknowledgements

This work was supported by start-up funding to MVS by the Bayer School of Natural and Environmental Science, Duquesne University. JO and GB are supported by the Nederlandse Organisatie voor Wetenschappelijk Onderzoek (NWO). Construction and shipping of the FT-ICR mass spectrometer was made possible through funding from the National High Field FT-ICR Facility (grant CHE-9909502) at the National High Magnetic Field Laboratory, Tallahassee, FL, USA. The excellent support by Dr B. Redlich and others of the FELIX staff is gratefully acknowledged.

REFERENCES

- [1] M. van Stipdonk, M. J. Kullman, G. Berden, J. Oomens. IRMPD and DFT study of the loss of water from protonated 2-hydroxynicotinic acid. *Int. J. Mass Spectrom.* **2012**, *330/332*, 134.
- [2] Z. N. Gaut, H. M. Solomon. Uptake and metabolism of nicotinic acid by human blood platelets. Effects of structure analogs and metabolic inhibitors. *Biochim. Biophys. Acta* **1970**, *201*, 316.
- [3] J. D. Hardy, H. G. Wolff, H. J. Goodell. Studies on pain. A new method for measuring pain threshold: observations on spatial summation of pain. *Clin. Invest.* **1940**, *19*, 649.
- [4] H. J. C. Tendeloo, F. W. Broekman, J. J. Stsiemlink. Analgesic and Antiphlogistic Compositions GB1362698, 1974-08-07; 1974.D
- [5] K. Moriya, K. Shibuya, Y. Hattori, S. Tsuboi, K. Shiokawa, S. Kagabu. 1-(6-Chloronicotiny)-2-nitroimino-imidazolidines and related compounds as potential new insecticides. *Biosci. Biotechnol. Biochem.* **1992**, *56*, 364.
- [6] K. Moriya, K. Shibuya, Y. Hattori, S. Tsuboi, K. Shiokawa, S. J. Kagabu. 1-Diazinylmethyl-2-nitromethylene-imidazolidines and 2-nitroimino-imidazolidines as new potential insecticides. *J. Pestic. Sci.* **1993**, *18*, 119.
- [7] K. Moriya, K. Shibuya, Y. Hattori, S. Tsuboi, K. Shiokawa, S. Kagabu. Imidacloprid and analogous insecticides. Part V. Structural modification of the 6-chloropyridyl moiety in the imidacloprid skeleton: Introduction of a five-membered heteroaromatic ring and the resulting insecticidal activity. *Biosci. Biotechnol. Biochem.* **1993**, *57*, 127.
- [8] R. C. Santos, R. M. B. M. Figueira, M. Fátima, M. Piedade, H. P. Diogo, M. E. Minas da Piedade. Energetics and structure of hydroxynicotinic acids. Crystal structures of 2-, 4-, 6-hydroxynicotinic and 5-chloro-6-hydroxynicotinic acids. *J. Phys. Chem. B* **2009**, *113*, 14291.
- [9] R. C. Dunbar. Photodissociation of trapped ions. *Int. J. Mass Spectrom.* **2000**, *200*, 571.
- [10] M. A. Duncan. Frontiers in the spectroscopy of mass-selected molecular ions. *Int. J. Mass Spectrom.* **2000**, *200*, 545.
- [11] N. C. Polfer, J. Oomens. Reaction products in mass spectrometry elucidated with infrared spectroscopy. *Phys. Chem.-Chem. Phys.* **2007**, *9*, 3804.
- [12] L. McAleese, P. Maitre. Infrared spectroscopy of organometallic ions in the gas phase: From model to real world complexes. *Mass Spectrom. Rev.* **2007**, *26*, 583.
- [13] G. S. Groenewold, J. Oomens, W. A. de Jong, G. L. Gresham, M. E. McIlwain, M. J. Van Stipdonk. Vibrational spectroscopy of anionic nitrate complexes of UO₂²⁺ and Eu³⁺ isolated in the gas phase. *Phys. Chem. Chem. Phys.* **2008**, *10*, 1192.
- [14] G. S. Groenewold, A. K. Gianotto, K. C. Cossel, M. J. Van Stipdonk, D. T. Moore, N. Polfer, J. Oomens, W. A. de Jong, L. Visscher. Vibrational spectroscopy of mass-selected

- [UO₂(ligand)_n]²⁺ complexes in the gas phase: comparison with theory. *J. Am. Chem. Soc.* **2006**, *128*, 4802.
- [15] G. S. Groenewold, A. K. Gianotto, K. C. Cossel, M. J. Van Stipdonk, J. Oomens, N. Polfer, D. T. Moore, W. A. de Jong, M. E. McIlwain. Mid-infrared vibrational spectra of discrete acetone-ligated cerium hydroxide cations. *Phys. Chem. Chem. Phys.* **2006**, *9*, 596.
- [16] G. S. Groenewold, A. K. Gianotto, M. E. McIlwain, M. J. Van Stipdonk, M. Kullman, D. T. Moore, N. Polfer, J. Oomens, I. Infante, L. Visscher, B. Siboulet, W. A. de Jong. Infrared spectroscopy of discrete uranyl anion complexes. *J. Phys. Chem. A* **2008**, *112*, 508.
- [17] G. S. Groenewold, M. J. Van Stipdonk, W. A. de Jong, J. Oomens, G. L. Gresham, M. E. McIlwain, D. Gao, B. Siboulet, L. Visscher, M. Kullman, N. Polfer. Infrared spectroscopy of dioxouranium(V) complexes with solvent molecules: Effect of reduction. *ChemPhysChem*. **2008**, *9*, 1278-1285.
- [18] J. J. Valle, J. R. Eyler, J. Oomens, D. T. Moore, A. F. G. van der Meer, G. von Helden, G. Meijer, C. L. Hendrickson, A. G. Marshall, G. T. Blakney. Free electron laser-Fourier transform ion cyclotron resonance mass spectrometry facility for obtaining infrared multiphoton dissociation spectra of gaseous ions. *Rev. Sci. Instrum.* **2005**, *76*, 023103.
- [19] V. N. Bagratashvili, V. A. Letokov, A. A. Makarov, E. A. Ryabov. *Multiple Photon Infrared Laser Photophysics and Photochemistry*. Harwood, Chur, Switzerland, **1985**.
- [20] D. T. Moore, J. Oomens, J. R. Eyler, G. von Helden, G. Meijer, R. C. Dunbar. Infrared spectroscopy of gas-phase Cr⁺ coordination complexes: Determination of binding sites and electronic states. *J. Am. Chem. Soc.* **2005**, *127*, 7243.
- [21] J. Oomens, A. G. G. M. Tielens, B. G. Sartakov, G. von Helden, G. Meijer. Laboratory infrared spectroscopy of cationic polycyclic aromatic hydrocarbon molecules. *Astrophys. J.* **2003**, *591*, 968.
- [22] M. J. Frisch, G. W. Trucks, H. B. Schlegel, G. E. Scuseria, M. A. Robb, J. R. Cheeseman, G. Scalmani, V. Barone, B. Mennucci, G. A. Petersson, H. Nakatsuji, M. Caricato, X. Li, H. P. Hratchian, A. F. Izmaylov, J. Bloino, G. Zheng, J. L. Sonnenberg, M. Hada, M. Ehara, K. Toyota, R. Fukuda, J. Hasegawa, M. Ishida, T. Nakajima, Y. Honda, O. Kitao, H. Nakai, T. Vreven, J. A. Montgomery Jr, J. E. Peralta, F. Ogliaro, M. Bearpark, J. J. Heyd, E. Brothers, K. N. Kudin, V. N. Staroverov, R. Kobayashi, J. Normand, K. Raghavachari, A. Rendell, J. C. Burant, S. S. Iyengar, J. Tomasi, M. Cossi, N. Rega, J. M. Millam, M. Klene, J. E. Knox, J. B. Cross, V. Bakken, C. Adamo, J. Jaramillo, R. Gomperts, R. E. Stratmann, O. Yazyev, A. J. Austin, R. Cammi, C. Pomelli, J. W. Ochterski, R. L. Martin, K. Morokuma, V. G. Zakrzewski, G. A. Voth, P. Salvador, J. J. Dannenberg, S. Dapprich, A. D. Daniels, Ö. Farkas, J. B. Foresman, J. V. Ortiz, J. Cioslowski, D. J. Fox. *Gaussian 09, Revision D.01*. Gaussian, Inc., Wallingford, CT, **2009**.
- [23] J. D. Steill, J. Oomens. Action spectroscopy of gas-phase carboxylate anions by multiple photon IR electron detachment/attachment. *J. Phys. Chem. A* **2009**, *113*, 4941.
- [24] J. D. Steill, J. Oomens. Free carboxylate stretching modes. *J. Phys. Chem. A* **2008**, *112*, 3281.
- [25] J. D. Steill, J. Oomens. Gas-phase deprotonation of p-hydroxybenzoic acid investigated by IR spectroscopy: Solution-phase structure is retained upon ESI. *J. Am. Chem. Soc.* **2009**, *131*, 13570.
- [26] R. Yamdagni, T. B. McMahon, P. Kebarle. Substituent effects on the intrinsic acidities of benzoic acids determined by gas phase proton transfer equilibria measurements. *J. Am. Chem. Soc.* **1974**, *96*, 4035.
- [27] T. B. McMahon, P. Kebarle. Intrinsic acidities of phenols and benzoic acids determined by gas-phase proton-transfer equilibria. *J. Am. Chem. Soc.* **1977**, *99*, 2222.
- [28] M. Fujio, R. T. McIver, R. W. Taft. Effects of the acidities of phenols from specific substituent-solvent interactions. Inherent substituent parameters from gas-phase acidities. *J. Am. Chem. Soc.* **1981**, *103*, 4017.
- [29] J. E. Bartmess, J. A. Scott, R. T. McIver. Substituent and solvation effects on gas-phase acidities. *J. Am. Chem. Soc.* **1979**, *101*, 6056.
- [30] D. Schroder, M. Budesínský, J. Roithova. Deprotonation of p-hydroxybenzoic acid: Does electrospray ionization sample solution or gas-phase structures? *J. Am. Chem. Soc.* **2012**, *134*, 15897.
- [31] Z. Tian, Z.-B. Wang, L.-S. Wang, S. R. Kass. Are carboxyl groups the most acidic sites in amino acids? Gas-phase acidity, photoelectron spectra, and computations on tyrosine, p-hydroxybenzoic acid and their conjugate bases. *J. Am. Chem. Soc.* **2009**, *131*, 1174.
- [32] M. Almasian, J. Grzetic, J. van Maurik, J. D. Steill, G. Berden, S. Ingemann, W. J. Buma, J. Oomens. Non-equilibrium isomer distribution of the gas-phase photoactive yellow protein chromophore. *J. Phys. Chem. Lett.* **2012**, *3*, 2259.

SUPPORTING INFORMATION

Additional supporting information may be found in the online version of this article at the publisher's website.